ACS SENSORS

pubs.acs.org/acssensors

Article

Parallel Field-Effect Nanosensors Detect Trace Biomarkers Rapidly at Physiological High-Ionic-Strength Conditions

Benjamin Barnes, Peng Wang, and YuHuang Wang*

Cite This: https://doi.org/10.1021/acssensors.2c00229

Read Online

ACCESS | Metrics & More | Article Recommendations | Supporting Information

ABSTRACT: Sensitivity and speed of detection are contradicting demands that profoundly impact the electrical sensing of molecular biomarkers. Although single-molecule sensitivity can now be achieved with single-nanotube field-effect transistors, these tiny sensors, with a diameter less than 1 nm, may take hours to days to capture the molecular target at trace concentrations. Here, we show that this sensitivity-speed challenge can be addressed using covalently functionalized double-wall CNTs that form many individualized, parallel pathways between two electrodes. Each carrier that travels across the electrodes is forced to take one of these pathways that are fully gated chemically by the target−probe binding events. This sensor design allows us to electrically detect Lyme disease oligonucleotide biomarkers directly at the physiological high-salt concentrations, simultaneously achieving both ultrahigh sensitivity (as low as 1 fM) and detection speed (<15 s). This unexpectedly simple strategy may open opportunities for sensor designs to broadly achieve instant detection of trace biomarkers and real-time probing of biomolecular functions directly at their physiological states.

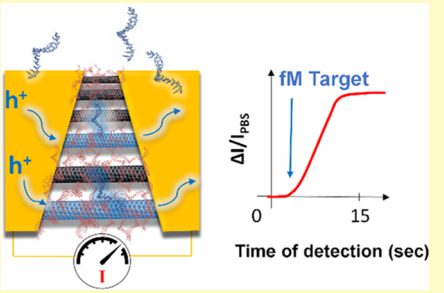

KEYWORDS: *double-wall carbon nanotube, Tube^2, point of care, field-effect transistor sensor, chemical gating, oligonucleotide detection, chemical detection*

Chemical sensors that can detect trace biomarkers rapidly, without the need of specialized equipment or laboratory processing, will enable timely detection[1] and longitudinal monitoring of diseases at the point of care[2] as well as real-time probing of biomolecular functions.[3] However, such sensors must overcome three major technical challenges: (1) the sensor must be sensitive and selective enough to detect the target analyte of interest;[4] (2) the detection must be sufficiently rapid, preferably on the order of minutes or even seconds;[5] and (3) the sensor should ideally function directly in the high-ionic-strength conditions of biofluids such as whole blood and saliva to minimize the requirement of sample processing steps[6] and more importantly, maximally preserve data relevance to the pristine physiological environment.[7] Additionally, such a device may allow real-time probing of biofunctions and enable efficient transduction of biochemical−electrical signals at the bioelectronics interface.[8,9]

Nanostructured field-effect transistor (FET) chemical sensors typically work by electrostatically gating their semiconducting channels with charged target molecules.[10,11] The probe molecules, such as oligonucleotides and antibodies, which are attached to the surface of the semiconducting device channel, selectively capture the target biomarkers to create a change in the local electrostatic field that modulates the electrical current passing through the device. FET sensors based on individual single-wall carbon nanotubes (CNTs) have demonstrated ultrahigh sensitivity, in some cases reaching the single-molecule limit for enzyme dynamics and DNA hybridization.[12−14] However, due to their small surface area, these tiny sensors, whose diameters are merely ∼1 nm, require extensive detection time (hours to days) to catch a target molecule at femtomolar concentrations.[5] In contrast, with a large sensor area, thin-film FETs can significantly accelerate the speed of detection and additionally benefit from simplified fabrication.[8,15] However, the sensitivity of thin-film FETs is typically much poorer than single-nanotube FETs.[15] Furthermore, electrical screening quickly dampens the electrostatic gating effect beyond the Debye length (λ_D), which is merely ∼0.8 nm in the high-ionic-strength conditions found in blood, saliva, or synovial fluid,[16,17] making it even more difficult to simultaneously achieve ultrahigh sensitivity and speed for electrical detection in pristine biofluids. Although there are clever tricks to circumvent some of these issues in specific use scenarios, this sensitivity-speed dilemma poses a fundamental challenge broadly impacting bioelectronics.

Here, we show that this sensitivity-speed challenge can be addressed by creating many nanoscale sensor pathways in parallel to simultaneously achieve ultrahigh sensitivity and instant detection, even under the physiological high-ionic-strength conditions (Figure 1). We assembled covalently

Received: January 28, 2022
Accepted: June 3, 2022

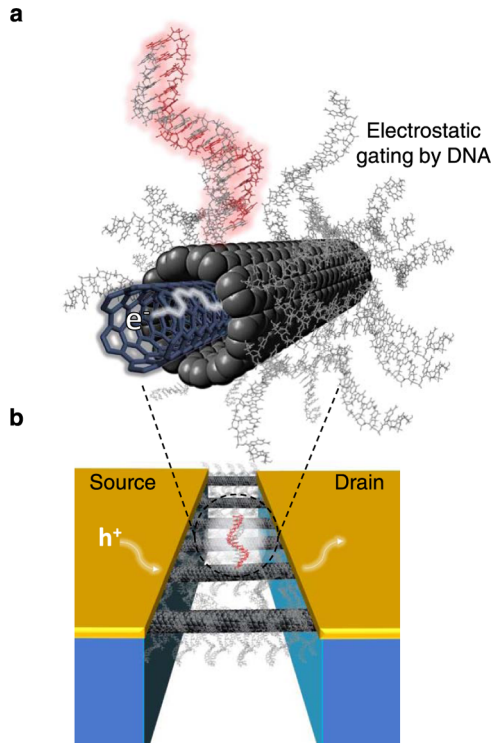

Figure 1. Covalently functionalized double-wall CNT field-effect biosensor with suspended and individualized parallel electrical pathways. (a) Schematic illustration of a single covalently functionalized double-wall CNT with the semiconducting inner-wall transporting charge carriers, and the outer-wall densely functionalized with DNA probe molecules. (b) Schematic of the aligned and suspended device architecture, consisting of individualized covalently functionalized double-wall CNTs aligned in parallel and suspended between two electrodes over a trench.

functionalized double-wall CNTs across a trench to form suspended individualized parallel pathways (SIP2) between a pair of gold electrodes. Each electrical pathway consists of a double-wall CNT densely functionalized with oligonucleotide probes covalently attached to the sensor surface. Electrical transport through the semiconducting inner tube is chemically gated by the target−probe interactions at the outer wall.[18] This covalently functionalized double-wall CNT (or "tube-in-a-tube") configuration provides a covalent functional layer that enables high selectivity and structural stability not possible with single-wall CNTs.[19] Since each covalently functionalized double-wall CNT spans the electrodes individually, it acts as a distinct electrical pathway that is comparable to a single-nanotube FET sensor, which has achieved single-molecule sensitivity.[12] By effectively increasing the sensor surface area with many of these nanosensors working in parallel, high speed of detection is realized while retaining the high sensitivity of individual single-wall CNT FET sensors. We note that although parallel aligned nanostructures are not "new," all previous studies, to the best of our knowledge, do not reveal this simple scaling relation that we found with the aligned and suspended device configuration for addressing these fundamental challenges in electrical detection. As a proof-of-concept application, we demonstrate the rapid detection of trace oligonucleotide biomarkers for Lyme disease, achieving instant detection with femtomolar sensitivity and two-mismatch selectivity, all directly at the physiological high ionic strengths.

RESULTS AND DISCUSSION

We fabricated aligned and suspended sensors from long double-wall CNTs that are attainable only recently using a nondestructive dispersion technique followed by length self-sorting, as we previously reported[20] (see the Materials and Methods for details). The double-wall CNTs used in this study have an average length of 1.85 μm, which is larger than a sonication control (0.44 μm), and 87% were longer than the trench width (1 μm) (Figure S1a). We used dielectrophoresis[21] to align the double-wall CNTs across two gold electrodes patterned on a p-doped silicon wafer with a 300 nm oxide layer. The doped silicon acts as a back gate allowing us to characterize the FET characteristics of the nanotubes but is not necessary for sensing. Dielectrophoresis is a promising technique for creating scalable sensing arrays.[22] The CNTs are aligned individually between the source and drain electrodes, with the number of nanotubes (2−100/device, up to 17 ± 3 pathways/μm) in each device consistently controlled through the magnitude and duration of the applied electric field (see the Materials and Methods section). Sensors used in the following experiments typically had 10 or fewer pathways. We note that long CNTs were essential for achieving aligned suspended channels, while shorter CNTs resulted in disordered networks and did not fully span the gap between the electrodes (Figure S1b−c). We attribute the improved alignment to a stronger dielectric force, which scales with the nanotube length,[21] that the longer double-wall CNTs experience compared with the short ones.

We then pinned the CNTs with gold top contacts, which define the source and drain electrodes, and etched the substrate oxide for 1 min with buffered hydrofluoric acid (6:1 volume ratio of 49% HF: 40% NH_4F) to create a 120 nm deep 1 μm wide trench underneath the CNTs, which removes the substrate effect and maximizes the exposed surface area of the sensors (see Figure S2 for the fabrication details). We used a trench width of 1 μm, as this distance could be routinely spanned by individual CNTs without dangling ends and when combined with top contacts, reduces the risk of CNTs collapsing into the trench. We then chemically functionalized the double-wall CNTs by reacting their outer walls with 2-fluorobenzoic acid diazonium salt.[18] We note that the outer layer serves as a functional layer that is complete and nonpermeable to small molecules as evidenced by the intactness of the inner tube under chemical attacks.[23] In this top-contacted configuration, the portion of the double-wall CNTs buried under the metal contact is protected from covalent functionalization allowing electrical contact to the tube-in-tube structure. The functionalization was followed by high-voltage electrical breakdown of those with metallic inner tubes, as previously described,[24] leaving most semiconducting walls intact (Figure S3a−b). Despite the high density of functional groups on the double-wall CNT surfaces, the inner tube remains chemically isolated from the outer wall-selective surface chemistry, therefore retaining its electrical conductivity (Figure S3a).[23] This approach provides a key advantage over other nanomaterials like single-wall CNTs and graphene, whose electrical properties degrade when covalently functionalized to a comparable degree.[25]

We investigated the sensing behavior of the aligned and suspended device through the electrical detection of model oligonucleotide biomarkers with a two-electrode device configuration. We note that Tube^2 field-effect sensors do

https://doi.org/10.1021/acssensors.2c00229
ACS Sens. XXXX, XXX, XXX−XXX

not require a gate electrode due to the electrostatic gating phenomenon we previously described.[18] We covalently linked the oligonucleotide probes (see Table S1 for the probe sequence) to the covalently functionalized double-wall CNTs through the surface 2-fluorobenzoic acid groups using the well-established carbodiimide cross-linking reaction.[18] We note that when carbodiimide cross-linking is used, normally it brings complexity to the sensor and the distance between the target molecular and channel increases, causing a decrease in sensitivity. In our case, the initial gap between the linker and semiconducting inner wall is less than a nanometer, so the small distance added by the linker does not significantly impact sensitivity. The oligonucleotide target we chose for this demonstration was a 30-base segment of a DNA biomarker for *Borrelia burgdorferi*, the bacterium that causes Lyme disease.[26] Prior to introducing the target molecules, we measured the current passing through the aligned and suspended device at a constant voltage bias of 0.5 V in 1X phosphate-buffered saline (PBS, containing 100 mM Na_3PO_4 and 150 mM NaCl) that mimics the high-salt physiological ionic conditions to determine the background signal and electrical noise. We measured the coefficient of variance of the electrical current over time for 13 devices and determined the average electrical noise to be 0.90 ± 1.01%. This small noise possibly originates from the interaction of the DNA probes, or ions from the buffer, with the semiconductor surface. However, this noise level is significantly smaller than the signal generated by the target analytes (discussed below) which was as much as 70%, allowing for sensitive chemical detection.

To determine the response time of the aligned and suspended sensor, we introduced 5 fM target DNA, also in 1X PBS, while applying 0.5 V across the source and drain electrodes. Within ∼2 s of adding the target, the device conductance increased by ∼50% and stayed constant (Figure 2a). The increasing current is due to the p-type behavior of the semiconducting double-wall CNTs, as the negative backbone of the DNA target is analogous to a negative gate bias. Previous molecular dynamics modeling with a single-wall CNT/DNA system confirms that the target−probe hybrid creates a high negative charge density near the CNT surface.[27] Of the 13 devices evaluated in this study, the response time was typically 1 to 15 s. While a rapid sensing response can also be achieved with randomly oriented covalently functionalized double-wall CNT films, the sensitivity of the SIP2 device configuration is significantly enhanced by about 6 orders of magnitude. In contrast, calculations based on the diffusion model predict that at femtomolar concentrations it would take hours for the first molecule to reach the surface of a single single-wall CNT.[5] The rapid response we observed with this device configuration is largely enabled by the greater (>20x) collective surface area, relative to a single single-wall CNT, of multiple long covalently functionalized double-wall CNTs acting in parallel, with additional contribution from the suspended structure which further increases surface area and enhances target−probe interactions. Finally, sensing in physiological-ionic-strength conditions lowers the energy threshold for target−probe DNA binding.

To determine the limit of detection and the dynamic range of this device configuration, we measured the signal of an aligned and suspended device while gradually increasing the target concentration (starting at 10^{-17} M) until we observed the conductance spike above the background noise. The detection limit was as low as 1 fM, with an average of 6 ± 5 fM

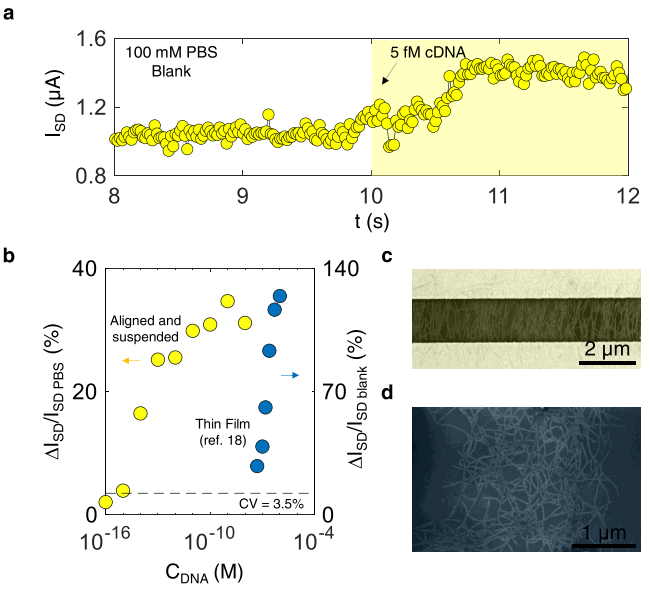

Figure 2. Electrical detection of an oligonucleotide Lyme disease biomarker. (a) Electrical current passing through the aligned and suspended device as a function of time at a constant voltage of 0.5 V. Note that the addition of 5 fM oligonucleotide target at t = 10 s led to an increase in the device conductance within just ∼2 s. (b) Current response of a representative sensor showing increasing conductance of the aligned and suspended device (yellow) and our previously demonstrated thin-film device (blue) as a function of target DNA concentration. Adapted with permission from ref 18. Copyright 2017 Journal of the American Chemical Society. Further reuse permissions should be requested from the American Chemical Society. https://pubs.acs.org/doi/10.1021/jacs.6b12111. (c) False-color SEM image of a device with a high density of covalently functionalized double-wall CNTs, which act as aligned electrical pathways. (d) False-color SEM image of a representative randomly oriented covalently functionalized double-wall CNT thin film.

from five devices evaluated on this parameter (Figure S4). This detection limit is comparable to state-of-the-art three-terminal field-effect sensors made from MoS_2 (with a detection limit of 6 fM)[28] and clustered regularly interspaced short palindromic repeats (CRISPR) technology-integrated graphene sensors (1.7 fM)[29] in similar ionic strength conditions. However, these devices require incubation times of 15 min to 1 h for the target and probe to hybridize. Additionally, unlike three-terminal FETs, our covalently functionalized double-wall CNT field-effect sensors enable efficient chemical gating in a simple two-terminal design, which significantly simplifies device fabrication. Furthermore, the dynamic range of these devices spanned from the fM to nM range (Figure 2b). This large dynamic range is a significant improvement over devices fabricated from thicker thin films, which have a dynamic range of just 10 nM to 1 μM.[18]

We attribute the improvement in both sensitivity and dynamic range to the SIP2 configuration, which confines the sensing current to parallel electrical pathways, each of which is fully gated by the target−probe interactions (Figure 2c). Since each electrical pathway directly bridges the electrodes, it is only necessary for target−probe interactions to occur on a single nanostructure for the device to be turned to a high-conductance ON-state. This mechanism contrasts with conventional thin-film devices where many nanostructures are not gated by the target−probe interactions due to leaky pathways, as typical with two-dimensional (2D) materials, or

https://doi.org/10.1021/acssensors.2c00229
ACS Sens. XXXX, XXX, XXX−XXX

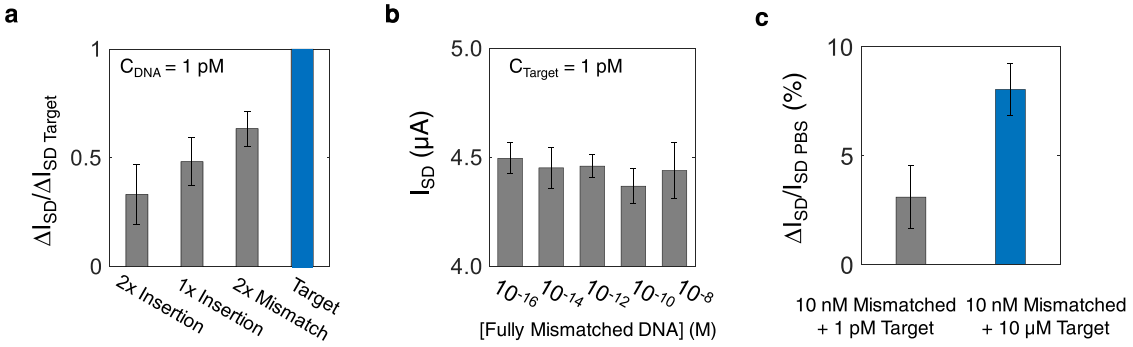

Figure 3. Aligned and suspended biosensors exhibit high selectivity for the target sequence. (a) Comparison of the current response of an aligned and suspended device for the target DNA, double-mismatch DNA, and DNA analytes offset by 1 and 2 inserted bases at a constant concentration of 1 pM at the high physiological ionic strength. The signals are normalized by the current response of the target sequence. Error bars represent the standard deviation between three different devices. (b) Aligned and suspended device current as a function of fully mismatched DNA concentration and a constant background concentration of 1 pM target DNA. Error bars represent 1 standard deviation. The signal was averaged over 50 s for each condition. (c) Comparison of the current response of the device in 10 nM mismatched DNA and 1 pM target (gray), and after spiking the sample with 10 μM target DNA (blue). Error bars represent 1 standard deviation. The signal was averaged over 50 s for each condition. The voltage was 0.5 V for all of the selectivity tests.

embedding in bundles. Furthermore, the aligned and suspended configuration, with its individualized electrical pathways, also contrasts with films composed of short covalently functionalized double-wall CNTs (Figure 2d) in which tube−tube junctions and semiconductor−substrate interactions can introduce electrical noise or crosstalk that obscure target−probe interactions at low concentrations.

In addition to high sensitivity and rapid response, high selectivity that allows us to distinguish between the target analyte and other similar molecules is required to prevent false-positive diagnoses. Lyme disease is an excellent example of this challenge. This disease affects 300,000 Americans annually and can cause long-term nerve and tissue damage without prompt detection and treatment.[26] However, its diagnosis currently relies on a two-step process that requires both enzyme-linked immunoassay and Western blotting to ensure selectivity and sensitivity.[26] The DNA from benign bacteria is also capable of binding to DNA probes for Lyme disease, which has led to false-positive diagnoses in previous polymerase chain reaction-based studies. To determine the selectivity of the aligned and suspended sensor design, we evaluated the device response to the target sequence and then to a benign bacteria DNA sequence that contains two mismatched bases, corresponding to a 6.9% mismatch, for a direct comparison (see Table S1 for the sequences). We found the current response of the double-base mismatch was only about 63% of that of the target (Figure 3a), demonstrating the ability to electronically distinguish between the two molecules. Additionally, we measured the device response to targets with 1 and 2 inserted bases that offset the sequence, which yielded signals of only ∼48 and ∼33% relative to the target analyte, respectively (Figure 3a). Swager and colleagues demonstrated high selectivity for DNA with a CNT nanowire sensor,[30] wherein the single-mismatch sequence only had an 80% response, and a double-mismatch sequence had a less than 10% response compared to the target. This high selectivity was facilitated with enzymatic metallization. Interestingly, the authors demonstrated temperature control as a means to achieving higher selectivity, observing a 30% response of the single mismatch compared to the target, by increasing the solution temperature from 25 to 32 °C, nearer the mismatch DNA melting point. This suggests a simple strategy of temperature control for improved selectivity in future applications with our device platform. While enzymatic metallization was shown to be an excellent approach for sensitive and selective DNA detection, the need for a 2 h incubation time and multiple rinsing and metallization steps introduces complexity into the device operation and precludes its use in real-time analyte monitoring, which is an area of future interest.

We further show this device configuration can also detect the target in the presence of other interfering molecules. We measured the response of an aligned and suspended device to a mixture of 1 pM target DNA and increasing concentrations of a fully mismatched 57-base DNA sequence (See Table S1 for details). Despite increasing the mismatched DNA concentration by 8 orders of magnitude, the signal did not increase (Figure 3b), indicating that nonspecific DNA interactions with our sensor are much smaller than those of the target DNA. To verify that the small amount of target DNA had not saturated the probes, thereby preventing nonspecific binding, we further spiked the sensor with 10 μM target DNA, which induced a 159% increase in the current response (Figure 3c). This signal spike ruled out the possibility of saturating the probes with the 1 pM target, unambiguously confirming that the signal modulation is dominated by the equilibrium between the probes and the target.

Since both selectivity and sensitivity are achieved in one test platform, this aligned and suspended device may provide a significant advantage over the traditional diagnostic approach for Lyme disease, which requires both enzyme-linked immunosorbent assay and Western blot analysis, but additional testing with clinical samples is needed to validate this hypothesis.[26] A one-step test that achieves both sensitivity and selectivity with high speed of detection, as we demonstrated here with aligned electrical pathways, could enable rapid diagnosis at the point of care, thus improving the outcomes of patients suspected of having Lyme disease.

The ability of the parallel pathway sensor to detect low analyte concentrations in 1X PBS, as demonstrated in the results above, is notable as this represents a physiological-ionic-strength condition with a short λ_D of merely 0.7 nm, which is shorter than the contour length of the DNA probes. Previously, it was demonstrated with streptavidin probes[31] and single-molecule DNA sensors[32] that the λ_D of the solution must be

https://doi.org/10.1021/acssensors.2c00229
ACS Sens. XXXX, XXX, XXX−XXX

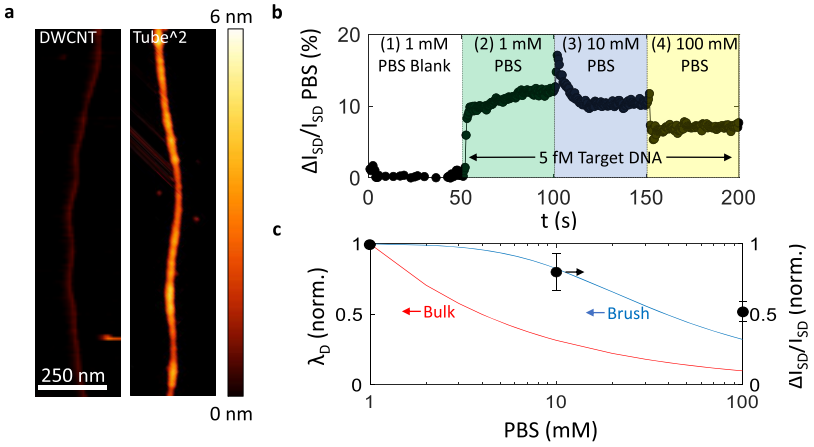

Figure 4. SIP2 devices maintain high signal transduction even at the high physiological ionic strength. (a) AFM micrographs of representative double-wall CNT before (left) and after (right) attaching probe DNA. The probe DNA packs densely on the covalently functionalized double-wall CNT surface adding an average height of 2.3 nm (measured in dry conditions). (b) Current response of an aligned and suspended device in four ionic strength regimes: blank media composed of 0.01X PBS (1); after 5 fM target DNA is added to the 0.01X PBS (2); and while the DNA target concentration is kept constant at 5 fM, PBS is increased to 0.1X (3) and 1X (4). (c) Comparison of the aligned and suspended device signal at a constant target DNA concentration of 5 fM (black) and λ_D of the bulk solution (red) and the predicted λ_D in the DNA brush (blue) as a function of the ionic strength (see the Supporting Information). The data points are normalized to the values at 0.01X PBS and averaged from three different devices. Error bars represent 1 standard deviation.

less than the height of the target−probe complex for a signal to be generated. Previous approaches to solve this include passivating the sensor surface with neutral polymers[17] using aptamer probes,[7,33] or controlling the orientation of binding molecules[34] but it is important to note that we do not use these strategies in this work. Instead, we hypothesize that the aligned suspended device's ability to sense in high-ionic-strength conditions results from the high density of probe molecules on the covalently functionalized double-wall CNT surface. Analytical modeling predicts that when DNA is grafted to a surface with a sufficient density, it forms a polymer brush that can exclude ions, reducing the local ionic strength compared to the bulk solution.[35] Our atomic force microscopy (AFM) studies indeed confirm that the DNA probes pack densely on the nanostructure surface (Figure 4a), which is consistent with brush formation. The average height of DNA on the covalently functionalized double-wall CNT surface was 2.3 ± 0.9 nm, with a maximum height of ∼5 nm (Figure S5). This height is smaller than the contour length of the DNA probes (∼9.9 nm)[36] probably because the AFM measurements were taken in dry conditions, and while there is also a possibility of the DNA wrapping the nanostructure, the result is comparable to previous studies of DNA brushes measured by AFM and ellipsometry.[37]

To determine if this brush structure contributes to the observed ability of the aligned suspended device to sense in high-ionic-strength conditions, we compared the scaling of the signal in different salt concentrations. Since the ionic strength in the brush structure decays more slowly than that in the bulk solution, we expect that the signal of the aligned and suspended sensor will decay as a function of the calculated local ionic strength in the brush instead of in the bulk solution. We measured the current response of an aligned and suspended device over time at 0.5 V in 0.01X, 0.1X, and 1X PBS while the target DNA concentration was maintained at 5 fM (Figure 4b) and compared it with the λ_D scaling from a theoretical model proposed by Schoning and colleagues to describe field-effect and capacitive sensing with DNA brushes (see the Supporting Information).[35] From 0.01X to 1X PBS, λ_D in the bulk solution decreased by 10-fold (from 7.6 to 0.76 nm), but the electrical response of the aligned suspended device decreased by only about 2-fold (Figure 4c). In this experiment, the device exhibited some electrical drift (Figure 4b). While the current gradually stabilizes, electrical drift remains a challenge in electrical biosensing that needs to be addressed in future work. This decay trend of the signal closely follows that predicted by the DNA brush model,[35] further supporting that the DNA probe brush structure contributes to the remarkable sensing performance in physiological salt concentrations observed in our aligned and suspended device. We note that previous work with wrinkled graphene has shown the importance of surface curvature on sensing in salty conditions, therefore the effect on sensing of the high curvature of the functionalized double-wall CNTs used in this work should be investigated in the future.[38]

We anticipate further development of this device configuration as the materials challenge is addressed. First, double-wall CNTs with semiconducting inner tubes[39] would be beneficial for optimizing the electrical transport properties of these devices. Despite the impressive performance of our aligned and suspended sensors, their ON/OFF ratios, between ∼50 and 300 (Figure S3a), are relatively low due to the presence of some metallic double-wall CNTs in our devices that are difficult to remove completely by electrical breakdown. However, even with this low ON/OFF ratio, we have observed detection limits down to 10^{-15} M, suggesting vast room for further improvement in ON/OFF ratio and sensitivity as pure semiconducting double-wall CNTs become attainable.[24,39] Second, large-scale fabrication of aligned and suspended devices will require a more scalable technique for aligning the double-wall CNTs, such as the recently discovered filtration method[40] if the technique can be scaled to the monolayer thickness for effective gating, or through the use of tangential flow-induced or DNA templated CNT self-assembly.[41,42]

https://doi.org/10.1021/acssensors.2c00229
ACS Sens. XXXX, XXX, XXX−XXX

CONCLUSIONS

We show that parallel and suspended covalently functionalized double-wall CNT field-effect sensors that form suspended, individualized parallel pathways (SIP2) can effectively address the sensitivity-speed challenge in the electrical detection of trace biomarkers. Compared to conventional thin films, SIP2 devices increase the sensitivity by approximately 6 orders of magnitude, demonstrating the significant benefits of restricting the electrical current to junction-free pathways that can be chemically gated. The collective sensing action of these parallel channels also enables fast detection (in seconds) by providing a relatively large surface area for sensing. Furthermore, the high density of probes on the covalently functionalized double-wall CNT surface contributes to sensing in high-ionic-strength conditions, with experimental evidence pointing to the formation of a DNA probe brush structure that locally excludes small ions. We demonstrate prototype devices targeting Lyme disease biomarkers, simultaneously achieving high sensitivity (as high as 1 fM), short detection time (<15 s), as well as high chemical selectivity, all directly at high physiological salt concentrations. Our result significantly simplifies Lyme disease diagnosis, which currently requires both enzyme-linked immunoassay and Western blotting to ensure selectivity and sensitivity, enabling a simple one-step diagnosis for this disease in contrast to the time-consuming and costly two-step process currently in use. Early and rapid detection of Lyme disease is just one example of the many applications that will be enabled by point-of-care electrical biosensors that can simultaneously overcome the key challenges of sensitivity, selectivity, response time, and ionic screening. The insight we have learned here may be broadly applicable to electrical detection based on the many varieties of low-dimensional materials.

MATERIALS AND METHODS

Dispersing and Sorting Ultralong Double-Wall CNTs. Ultralong double-wall CNTs were separated from raw materials using a length self-sorting method as we previously reported.[20] Briefly, DWCNT powder (Cheap Tubes) was dissolved in chlorosulfonic acid (99%, MilliporeSigma) at a concentration of 1 mg/mL and then dispersed in 0.08 wt % sodium deoxycholate (DOC, >97%, MilliporeSigma) and 0.75 M NaOH. The double-wall CNTs and sodium deoxycholate were precipitated by adding 37% HCl, typically 1−3 mL, to lower the pH to below the pK_a of DOC (pH ∼6.6), and then redispersed with 1 M NaOH (to increase the pH above 6.6) to a final surfactant concentration of 6 wt %. The suspension was centrifuged at 16,400 rpm for 90 min to separate both long and short double-wall CNTs. The precipitated long double-wall CNTs were washed with nanopure water and isopropanol, dried, and redissolved in chlorosulfonic acid at 0.7 mg/mL, after which the dispersal in sodium deoxycholate and NaOH was conducted again. The process was repeated 2 more times (for a total of 4 length sorting cycles) at DWCNT concentrations of 0.5 and 0.1 mg/mL in chlorosulfonic acid, respectively, to further enrich the population of long double-wall CNTs. The final DWCNT suspension contained 5 wt % sodium deoxycholate.

Diazonium Salt Synthesis. 2-Fluorobenzoic acid diazonium tetrafluoroborate was synthesized according to a previous procedure.[18] Briefly, 4.814 mmol of 4-amino-2-fluorobenzoic acid (TCI) was added to 3 mL of nanopure water in a round-bottom flask fully covered in aluminum foil to prevent light exposure, which was then submerged in an ice bath. Next, 2.68 mL of fluoroboric acid (48 wt %; MilliporeSigma) was added to the flask while stirring. Sodium nitrite (670 mg) was dissolved in 2 mL of nanopure water and added to the round-bottom flask dropwise. The solution was stirred in the dark for 15 min, after which the solid product was collected on a PTFE filtration membrane and rinsed with ∼100 mL of diethyl ether. The product was then dried in the dark for 20 min under vacuum and stored in the dark in a sealed vial at 0 °C.

Fabrication of Aligned and Suspended Covalently Functionalized Double-Wall CNT Semiconductors. As shown in Figure S2, phosphorous-doped silicon wafers (1−10 Ω cm) with a 300 nm thermal oxide layer (University Wafer) were cleaned in piranha solution (3:1 by volume H_2SO_4:H_2O_2 (30 wt %)), rinsed copiously with nanopure water and isopropanol, and finally blown dry with compressed nitrogen. A positive photoresist (Shipley 1813) was used to pattern dielectrophoresis electrodes with a 5 μm channel. A chromium/gold (10/30 nm) bilayer was deposited using thermal evaporation at 10^{-7} Torr. The excess metal was lifted off in Remover PG at 80 °C for 30 min. Before use, the electrodes were rinsed again with water and acetone and blown dry.

Pristine double-wall CNTs were deposited using a dielectrophoresis procedure[21] using the previously fabricated electrodes and the length-sorted aqueous suspension of double-wall CNTs in sodium deoxycholate, diluted 10x with Nanopure water. To obtain only a few individualized double-wall CNTs per device, we used the following dielectrophoresis parameters: 10 MHz, 5 V amplitude, and 1−4 min of applied voltage. After dielectrophoresis alignment, the device was coated with electron beam resist (PMMA 495K) and a second pair of electrodes (top contacts) was defined on top of the previous electrodes using electron beam lithography (Raith e-line), which were 10 μm wide and separated by a 1 μm gap. Cr/Au (5/20 nm) was deposited over the patterned substrate, yielding a 1 μm channel in the final device with 2 μm of both ends of the double-wall CNTs buried beneath the top contacts. The top contacts prevent short double-wall CNTs that do not span the channel from contributing to electrical noise, as well as anchor the double-wall CNTs to keep them from collapsing during wet etching of the silicon wafer. The aligned double-wall CNTs exhibited low resistance and an ON/OFF current ratio of ∼1 (Figure S3a) due to the presence of some metallic inner and outer carbon nanotubes. Raw double-wall CNTs typically consist of a mixture of semiconducting and metallic outer walls and inner walls. We partially etched away the substrate oxide using a 6:1 HF/NH_4F buffered oxide etchant to create a 120 nm deep trench in between the source and drain electrodes. Immediately after etching, the devices were dried using supercritical CO_2 (Tousimis).

The double-wall CNTs were covalently functionalized *in situ* using 2-fluorobenzoic acid diazonium salt by submerging the devices in 1 mM diazonium salt solution for 12 h, followed by 10 mM diazonium salt for 12 h. The reactions were conducted in the dark. After the reaction time, the devices were rinsed with nanopure water to remove the unreacted diazonium salt.

The metallic inner carbon nanotubes were then destroyed using electrical breakdown. In this process, the source−drain voltage was increased from 0 V until a sharp spike in resistance was observed, indicating that one metallic carbon nanotube was destroyed. Breakdown typically occurred between 10 and 20 V. This was repeated until the ON/OFF ratio reached 10−1000 (Figure S3a). What remained were individual pristine semiconducting nanotubes sealed inside insulating outer walls that are covalently grafted with a layer of aryl groups terminated with COOH functional groups.

We then covalently attached 30-base ssDNA probes with 5′ amino termini (Integrated DNA Technologies) to the surface carboxyl groups on the covalently functionalized double-wall CNTs using a previous method.[18] Briefly, the carboxyl groups were activated in 0.4 mg/mL 1-ethyl-3-(3-(dimethylamino)propyl)carbodiimide and 1.01 mg/mL sulfo-*N*-hydroxysuccinimide in 10 mM MES (Covachem) for 15 min. Amino-terminated ssDNA probes were then attached to the activated groups by placing a droplet of 10 μM of ssDNA in 0.1X PBS (CovaChem, LLC) on the device. The ssDNA solution was replaced by a pipette on the device every 15 min for 1 h. The devices were then rinsed with nanopure water and stored in 1x PBS (1x PBS was prepared by the instructions provided by CovaChem and consisted of 100 mM sodium phosphate and 150 mM sodium chloride) until characterization (within 1 day of fabrication).

https://doi.org/10.1021/acssensors.2c00229
ACS Sens. XXXX, XXX, XXX−XXX

Electrical Characterization. The *I*−*V*, transconductance, and sensing curves were collected using a Keithley 4200 Semiconductor Parameter Analyzer. Typical sensing experiments were conducted by placing a 10 μL droplet of the oligonucleotide analyte in PBS on the device channel and either sweeping the source−drain voltage between −1 and 1 V, or by measuring the current over time with an applied bias of 0.5 V. No appreciable evaporation of the droplet was observed during the short testing period, and the temperature and relative humidity were maintained in the lab across all experiments. Noise was quantified by calculating the coefficient of variation of the current in buffer. Sensing measurements were always conducted from blank PBS to increasing analyte concentrations. Sensing curves were reported as the % change in current (with respect to the blank measurement) at 0.5 V unless specified otherwise in the text. The device channel was not allowed to dry at any time during the sensing characterization.

AFM Characterization. Freshly cleaved mica substrates were soaked in 1 M magnesium sulfate for 10 min, blown dry with compressed nitrogen, and rinsed with nanopure water. The solution of length-sorted double-wall CNTs dispersed in sodium deoxycholate was then dropped onto the mica surface and allowed to incubate for 10 min, after which the droplet was blown away. The substrate was then rinsed with water and blown dry. The double-wall CNTs and covalently functionalized double-wall CNTs were characterized in tapping mode using a Cypher ES AFM (Asylum Research Corporation) with gold back side-coated AFM probes (Tap300GD-G, force constant = 40 N m^{-1}, BudgetSensors).

Raman Characterization. Raman scattering was measured directly on aligned and suspended devices with a Horiba Aramis Raman microscope at an excitation wavelength of 532 nm. The Raman shift was calibrated with a silicon chip. A 50x microscope objective and line scan were used to collect up to 10 spectra from between the electrodes where the double-wall CNTs or covalently functionalized double-wall CNTs were located.

■ ASSOCIATED CONTENT

Supporting Information

The Supporting Information is available free of charge at https://pubs.acs.org/doi/10.1021/acssensors.2c00229.

> Length-sorted double-wall CNTs enabling the fabrication of aligned and suspended devices (Figure S1); schematic of device fabrication, electrical properties, and Raman analysis during covalent modification of double-wall CNTs (Figure S2); test data from the five devices used to determine detection limit and dynamic range (Figure S3); topographical height profile of a double-wall CNT compared with a covalently functionalized double-wall CNT after attaching DNA probes (Figure S4); and ionic strength model of the DNA brush structure (Figure S5); and oligonucleotide probe, target, and mismatch sequences used in this study (Table S1) (PDF)

■ AUTHOR INFORMATION

Corresponding Author

YuHuang Wang − *Department of Chemistry and Biochemistry and Maryland NanoCenter, University of Maryland, College Park, Maryland 20742, United States;* orcid.org/0000-0002-5664-1849; Email: yhw@umd.edu

Authors

Benjamin Barnes − *Department of Chemistry and Biochemistry and Department of Materials Science and Engineering, University of Maryland, College Park, Maryland 20742, United States;* orcid.org/0000-0002-0865-8486

Peng Wang − *Department of Chemistry and Biochemistry, University of Maryland, College Park, Maryland 20742, United States;* orcid.org/0000-0003-0343-3920

Complete contact information is available at: https://pubs.acs.org/10.1021/acssensors.2c00229

Author Contributions

B.B. and Y.H.W. conceived the idea, designed experiments, and analyzed the data. P.W. sorted nanotubes, and B.B. performed device fabrication, surface functionalization, electrical characterization, as well as all of the other experiments. B.B. and Y.H.W. wrote the manuscript with inputs from all authors.

Notes

The authors declare no competing financial interest.

All data needed to evaluate the conclusions in the paper are present in the paper and/or the Supporting Information.

■ ACKNOWLEDGMENTS

Funding: Research reported in this publication was supported in part by the National Institute of General Medical Sciences of the National Institutes of Health under Award Number R01GM114167. The content is solely the responsibility of the authors and does not necessarily represent the official views of the National Institutes of Health. The authors also gratefully acknowledge the National Science Foundation for supporting the shared AFM shared system (MRI Program grant no. CHE1626288) through which the AFM images were obtained and for developing the diazonium chemistry which is applied here (grant no. CHE1904488).

■ REFERENCES

(1) Gubala, V.; Harris, L. F.; Ricco, A. J.; Tan, M. X.; Williams, D. E. Point of Care Diagnostics: Status and Future. *Anal. Chem.* **2012**, *84*, 487−515.

(2) Gambhir, S. S.; Ge, T. J.; Vermesh, O.; Spitler, R. Toward achieving precision health. *Sci. Transl. Med.* **2018**, *10*, No. eaao3612.

(3) Akkilic, N.; Geschwindner, S.; Höök, F. Single-molecule biosensors: Recent advances and applications. *Biosens. Bioelectron.* **2020**, *151*, No. 111944.

(4) Turner, A. P. F. Biosensors: Sense and Sensibility. *Chem. Soc. Rev.* **2013**, *42*, 3184−3196.

(5) Sheehan, P. E.; Whitman, L. J. Detection Limits for Nanoscale Biosensors. *Nano Lett.* **2005**, *5*, 803−807.

(6) Vashist, S. K.; Luppa, P. B.; Yeo, L. Y.; Ozcan, A.; Luong, J. H. T. Emerging Technologies for Next-Generation Point-of-Care Testing. *Trends Biotechnol.* **2015**, *33*, 692−705.

(7) Nakatsuka, N.; Yang, K.-A.; Abendroth, J. M.; Cheung, K. M.; Xu, X.; Yang, H.; Zhao, C.; Zhu, B.; Rim, Y. S.; Yang, Y.; Weiss, P. S.; Stojanovich, M. N.; Andrews, A. M. Aptamer−Field-Effect Transistors Overcome Debye Length Limitations for Small-Molecule Sensing. *Science* **2018**, *362*, 319−324.

(8) Cao, Q.; Rogers, J. A. Ultrathin films of single-walled carbon nanotubes for electronics and sensors: A review of fundamental and applied aspects. *Adv. Mater.* **2009**, *21*, 29−53.

(9) Li, P.; Lee, G.-H.; Kim, S. Y.; Kwon, S. Y.; Kim, H.-R.; Park, S. From Diagnosis to Treatment: Recent Advances in Patient-Friendly Biosensors and Implantable Devices. *ACS Nano* **2021**, *15*, 1960−2004.

(10) Béraud, A.; Sauvage, M.; Bazán, C. M.; Tie, M.; Bencherif, A.; Bouilly, D. Graphene field-effect transistors as bioanalytical sensors: design, operation and performance. *Analyst* **2021**, *146*, 403−428.

(11) Stern, E.; Klemic, J. F.; Routenberg, D. A.; Wyrembak, P. N.; Turner-Evans, D. B.; Hamilton, A. D.; LaVan, D. A.; Fahmy, T. M.; Reed, M. A. Label-Free Immunodetection with CMOS-Compatible Semiconducting Nanowires. *Nature* **2007**, *445*, 519−522.

(12) Choi, Y.; Moody, I. S.; Sims, P. C.; Hunt, S. R.; Corso, B. L.; Perez, I.; Weiss, G. A.; Collins, P. G. Single-Molecule Lysozyme Dynamics Monitored by an Electronic Circuit. *Science* **2012**, *335*, 319−324.
(13) Sorgenfrei, S.; Chiu, C.-y.; Gonzalez, R. L.; Yu, Y.-J.; Kim, P.; Nuckolls, C.; Shepard, K. L. Label-free single-molecule detection of DNA-hybridization kinetics with a carbon nanotube field-effect transistor. *Nat. Nanotechnol.* **2011**, *6*, 126−132.
(14) Vernick, S.; Trocchia, S. M.; Warren, S. B.; Young, E. F.; Bouilly, D.; Gonzalez, R. L.; Nuckolls, C.; Shepard, K. L. Electrostatic melting in a single-molecule field-effect transistor with applications in genomic identification. *Nat. Commun.* **2017**, *8*, No. 15450.
(15) Schroeder, V.; Savagatrup, S.; He, M.; Lin, S.; Swager, T. M. Carbon Nanotube Chemical Sensors. *Chem. Rev.* **2019**, *119*, 599−663.
(16) Israelachvili, J. N. *Intermolecular and Surface Forces*, 3rd ed.; Academic Press: Burlington, 2011.
(17) Gao, N.; Gao, T.; Yang, X.; Dai, X.; Zhou, W.; Zhang, A.; Lieber, C. M. Specific Detection of Biomolecules in Physiological Solutions Using Graphene Transistor Biosensors. *Proc. Natl. Acad. Sci. U.S.A.* **2016**, *113*, 14633−14638.
(18) Ng, A. L.; Chen, C.-F.; Kwon, H.; Peng, Z.; Lee, C. S.; Wang, Y. Chemical Gating of a Synthetic Tube-in-a-Tube Semiconductor. *J. Am. Chem. Soc.* **2017**, *139*, 3045−3051.
(19) Huang, J.; Ng, A. L.; Piao, Y.; Chen, C.-F.; Green, A. A.; Sun, C.-F.; Hersam, M. C.; Lee, C. S.; Wang, Y. Covalently Functionalized Double-Walled Carbon Nanotubes Combine High Sensitivity and Selectivity in the Electrical Detection of Small Molecules. *J. Am. Chem. Soc.* **2013**, *135*, 2306−2312.
(20) Wang, P.; Barnes, B.; Wu, X.; Qu, H.; Zhang, C.; Shi, Y.; Headrick, R. J.; Pasquali, M.; Wang, Y. Self-Sorting of 10-μm-Long Single-Walled Carbon Nanotubes in Aqueous Solution. *Adv. Mater.* **2019**, *31*, No. 1901641.
(21) Duchamp, M.; Lee, K.; Dwir, B.; Seo, J. W.; Kapon, E.; Forro, L.; Magrez, A. Controlled Positioning of Carbon Nanotubes by Dielectrophoresis: Insights into the Solvent and Substrate Role. *ACS Nano* **2010**, *4*, 279−284.
(22) Xu, X.; Clément, P.; Eklöf-Österberg, J.; Kelley-Loughnane, N.; Moth-Poulsen, K.; Chávez, J. L.; Palma, M. Reconfigurable Carbon Nanotube Multiplexed Sensing Devices. *Nano Lett.* **2018**, *18*, 4130−4135.
(23) Piao, Y.; Chen, C.-F.; Green, A. A.; Kwon, H.; Hersam, M. C.; Lee, C. S.; Schatz, G. C.; Wang, Y. Optical and Electrical Properties of Inner Tubes in Outer Wall-Selectively Functionalized Double-Wall Carbon Nanotubes. *J. Phys. Chem. Lett.* **2011**, *2*, 1577−1582.
(24) Ng, A. L.; Sun, Y.; Powell, L.; Sun, C.-F.; Chen, C.-F.; Lee, C. S.; Wang, Y. Selective Breakdown of Metallic Pathways in Double-Walled Carbon Nanotube Networks. *Small* **2015**, *11*, 96−102.
(25) Bouilly, D.; Cabana, J.; Meunier, F.; Desjardins-Carrière, M.; Lapointe, F.; Gagnon, P.; Larouche, F. L.; Adam, E.; Paillet, M.; Martel, R. Wall-Selective Probing of Double-Walled Carbon Nanotubes Using Covalent Functionalization. *ACS Nano* **2011**, *5*, 4927−4934.
(26) Steere, A. C.; Strle, F.; Wormser, G. P.; Hu, L. T.; Branda, J. A.; Hovius, J. W. R.; Li, X.; Mead, P. S. Lyme borreliosis. *Nat. Rev. Dis. Primers* **2016**, *2*, No. 16090.
(27) Côté, S.; Bouilly, D.; Mousseau, N. The molecular origin of the electrostatic gating of single-molecule field-effect biosensors investigated by molecular dynamics simulations. *Phys. Chem. Chem. Phys.* **2022**, *24*, 4174−4186.
(28) Mei, J.; Li, Y.-T.; Zhang, H.; Xiao, M.-M.; Ning, Y.; Zhang, Z.-Y.; Zhang, G. J. Molybdenum Disulfide Field-Effect Transistor Biosensor for Ultrasensitive Detection of DNA by Employing Morpholino as Probe. *Biosens. Bioelectron.* **2018**, *110*, 71−77.
(29) Hajian, R.; Balderston, S.; Tran, T.; deBoer, T.; Etienne, J.; Sandhu, M.; Wauford, N. A.; Chung, J.-Y.; Nokes, J.; Athaiya, M.; Paredes, J.; Peytavi, R.; Goldsmith, B.; Murthy, N.; Conboy, I. M.; Aran, K. Detection of Unamplified Target Genes Via CRISPR−Cas9 Immobilized on a Graphene Field-Effect Transistor. *Nat. Biomed. Eng.* **2019**, *3*, 427−437.
(30) Weizmann, Y.; Chenoweth, D. M.; Swager, T. M. DNA−CNT Nanowire Networks for DNA Detection. *J. Am. Chem. Soc.* **2011**, *133*, 3238−3241.
(31) Stern, E.; Wagner, R.; Sigworth, F. J.; Breaker, R.; Fahmy, T. M.; Reed, M. A. Importance of the Debye Screening Length on Nanowire Field Effect Transistor Sensors. *Nano Lett.* **2007**, *7*, 3405−3409.
(32) Sorgenfrei, S.; Chiu, C.-y.; Johnston, M.; Nuckolls, C.; Shepard, K. L. Debye Screening in Single-Molecule Carbon Nanotube Field-Effect Sensors. *Nano Lett.* **2011**, *11*, 3739−3743.
(33) Zheng, H. Y.; Alsager, O. A.; Zhu, B.; Travas-Sejdic, J.; Hodgkiss, J. M.; Plank, N. O. V. Electrostatic gating in carbon nanotube aptasensors. *Nanoscale* **2016**, *8*, 13659−13668.
(34) Xu, X.; Bowen, B. J.; Gwyther, R. E. A.; Freeley, M.; Grigorenko, B.; Nemukhin, A. V.; Eklöf-Österberg, J.; Moth-Poulsen, K.; Jones, D. D.; Palma, M. Tuning Electrostatic Gating of Semiconducting Carbon Nanotubes by Controlling Protein Orientation in Biosensing Devices. *Angew. Chem., Int. Ed.* **2021**, *60*, 20184−20189.
(35) Poghossian, A.; Cherstvy, A.; Ingebrandt, S.; Offenhäusser, A.; Schöning, M. J. Possibilities and Limitations of Label-Free Detection of DNA Hybridization With Field-Effect-Based Devices. *Sens. Actuators, B* **2005**, *111−112*, 470−480.
(36) Damaschun, G.; Damaschun, H.; Misselwitz, R.; Pospelov, V. A.; Zalenskaya, I. A.; Zirwer, D.; Müller, J. J.; Vorobev, V. I. How Many Base-Pairs Per Turn Does DNA Have in Solution and in Chromatin? An Answer from Wide-Angle X-Ray Scattering. *Biomed. Biochim. Acta* **1983**, *42*, 697−703.
(37) Legay, G.; Markey, L.; Meunier-Prest, R.; Finot, E. Measurements of Thickness Dispersion in Biolayers by Scanning Force Microscopy and Comparison with Spectroscopic Ellipsometry Analysis. *Ultramicroscopy* **2007**, *107*, 1111−1117.
(38) Hwang, M. T.; Heiranian, M.; Kim, Y.; You, S.; Leem, J.; Taqieddin, A.; Faramarzi, V.; Jing, Y.; Park, I.; van der Zande, A. M.; Nam, S.; Aluru, N. R.; Bashir, R. Ultrasensitive detection of nucleic acids using deformed graphene channel field effect biosensors. *Nat. Commun.* **2020**, *11*, No. 1543.
(39) Li, H.; Gordeev, G.; Wasserroth, S.; Chakravadhanula, V. S. K.; Neelakandhan, S. K. C.; Hennrich, F.; Jorio, A.; Reich, S.; Krupke, R.; Flavel, B. S. Inner- and Outer-Wall Sorting of Double-Walled Carbon Nanotubes. *Nat. Nanotechnol.* **2017**, *12*, 1176−1182.
(40) He, X.; Gao, W.; Xie, L.; Li, B.; Zhang, Q.; Lei, S.; Robinson, J. M.; Hároz, E. H.; Doorn, S. K.; Wang, W.; Vajtai, R.; Ajayan, P. M.; Adams, W. W.; Hauge, R. H.; Kono, J. Wafer-scale monodomain films of spontaneously aligned single-walled carbon nanotubes. *Nat. Nanotechnol.* **2016**, *11*, 633−638.
(41) Sun, W.; Shen, J.; Zhao, Z.; Arellano, N.; Rettner, C.; Tang, J.; Cao, T.; Zhou, Z.; Ta, T.; Streit, J. K.; Fagan, J. A.; Schaus, T.; Zheng, M.; Han, S.-J.; Shih, W. M.; Maune, H. T.; Yin, P. Precise pitch-scaling of carbon nanotube arrays within three-dimensional DNA nanotrenches. *Science* **2020**, *368*, 874−877.
(42) Jinkins, K. R.; Foradori, S. M.; Saraswat, V.; Jacobberger, R. M.; Dwyer, J. H.; Gopalan, P.; Berson, A.; Arnold, M. S. Aligned 2D carbon nanotube liquid crystals for wafer-scale electronics. *Sci. Adv.* **2021**, *7*, No. eabh0640.

https://doi.org/10.1021/acssensors.2c00229
ACS Sens. XXXX, XXX, XXX−XXX